Improving the performance of low-frequency magnetic energy harvesters using an internal magnetic-coupled mechanism

Zhixiong You,[1] Huining Miao,[1] Yang Shi,[1,a)] and Michael Beer[2,3,4]

[1]Research Center for Applied Mechanics, School of Mechano-Electronic Engineering, Xidian University, Xi'an 710071, China

[2]Institute for Risk and Uncertainty, University of Liverpool, Liverpool, UK

[3]Institute for Risk and Reliability, Leibniz University Hannover, Hannover, Germany

[4]International Joint Research Center for Resilient Infrastructure & International Joint Research Center for Engineering Reliability and Stochastic Mechanics, Tongji University, Shanghai, China

Abstract

In this study, we present a novel low-frequency magnetic field energy harvester (EH) employing beryllium bronze/Pb(Zr,Ti)O_3 ceramic composited dual-beam structures with tip magnets attached to the inner and outer beams. This design incorporates the internal magnetic-coupled (IMC) effect, resulting in significantly enhanced coupling ability and a wide bandwidth. The validity of the IMC mechanism is confirmed through theoretical formulas and numerical simulations. By leveraging the IMC condition, the EH achieves an expanded bandwidth, increasing from 22 Hz to 43 Hz. Moreover, the total output voltages at the inherent resonance and internal resonance are boosted by 15.4% and 32%, respectively. The performance of the IMC-EH can be further improved by increasing the number of the endmost magnets. Experimental investigations reveal that the IMC-EH generates a maximum RMS output power density of 56.25 $\mu W \cdot Oe^{-2} \cdot cm^{-3}$, surpassing existing magnetically coupled piezoelectric energy harvesters. Remarkably, even under an ambient magnetic field as low as 1 Oe, the proposed IMC-EH still yields a total output power of 185 μW, sufficient to continuously power 26 LEDs in real-time. This demonstrates its potential as a promising solution for low-power consumption small electronics. Furthermore, the implications of this work extend beyond its immediate benefits, as it inspires the design of future self-powered wireless sensor networks in the context of the Internet of Things.

Keywords: magnetic energy harvesters; internal magnetic-coupled; inherent resonance; bandwidth.

1. Introduction

With the rapid development of the Internet of Things (IoT), wireless sensor networks have become extensively utilized in various aspects of human life and production. However, ensuring a stable power supply for wireless sensor nodes remains a challenge. Currently, traditional chemical batteries are primarily used to power wireless sensor nodes. However, these batteries have limited lifespans, contribute to environmental pollution, and impose significant constraints. As a result, researchers have shifted their focus to exploring alternative power supply solutions based on environmental energy sources such as wind energy, solar energy, vibrations, and stray magnetic fields.[1,2] Among these options, harnessing magnetic energy from the natural environment shows the most promising potential for powering wireless sensor nodes and miniaturized low-power electronics. This is because we are constantly surrounded by stray magnetic fields, typically below 10 Oe at a fixed frequency, induced from electric cables.[3-5]

To date, magneto-mechano-electric (MME) harvesters have emerged as a promising solution for standalone-powered IoT systems. These harvesters utilize various energy conversion components, including piezoelectric, magnetostrictive, triboelectric materials, and magnets. The primary function of MME harvesters is to convert AC magnetic fields into mechanical vibrations through the magnetostrictive effect or magnetic force. Subsequently, these vibrations are converted into an electric field using the piezoelectric or triboelectric effect.[6-8] The MME system typically consists of a piezoelectric layer, an elastic layer, and tip magnets, enabling simultaneous harvesting of low-frequency magnetic fields and mechanical vibrations.[9,10] Yu et al.[11] designed an MME energy harvester using a trapezoidal Ni/PZT cantilever beam, which exhibited enhanced coupling with very weak magnetic fields due to the dual effects of stress concentration and magnetic flux concentration. This design achieved a maximum output power density of 7.16 $\mu W \cdot Hz^{-1} \cdot Oe^{-2} \cdot cm^{-3}$. Gao et al.[12] proposed a hybrid multi-mode energy harvester based on Metglas/PMN-PT composites. By fixing three piezoelectric sheets on a cantilever beam, they achieved a maximum output power of 50 μW/Oe. Liu et al.[13] designed an MME composite consisting of piezoelectric bimorphs and a tip magnet. This design exhibited a maximum power density of 11.73

$\mu W \cdot Oe^{-2} \cdot cm^{-3}$ when subjected to low-frequency (< 100 Hz) magnetic fields. The conventional MME harvesters have limited available energy conversion efficiency only around their resonance frequency, which restricts their applicability in environments with stray magnetic fields due to their narrow bandwidth. To address this issue, researchers have proposed nonlinear energy harvesters (EHs) based on bi-stable,[14,15] tri-stable vibration,[16-19] and multi-frequency modes.[20] The design of multi-stable EHs involves magnetic coupling between the endmost magnets and external magnets. Song et al.[21] designed a magnetic-coupled piezoelectric energy harvester array that demonstrated dual-mode energy harvesting capabilities, achieving a maximum output power density of 36.5 $\mu W \cdot Oe^{-2} \cdot cm^{-3}$ under ambient magnetic fields. Haghighi et al.[22] investigated magnetically coupled piezoelectric beam arrays and found that the multi-frequency nonlinear structure improved the efficiency and bandwidth of energy harvesting. Liu et al.[23] developed an I-L type magnetic-coupled piezoelectric energy harvester by introducing nonlinear magnetic forces. They modified the output characteristics by adjusting the distance between the two magnets. While previously reported nonlinear EHs have supplied a few μW/mW-scale energy to simple function IoT sensors, this level of power may not be sufficient for integrated devices, as many of them have complex structures that are not suitable for small electronic devices.

In this study, we present a novel approach to broaden the frequency band of EHs by utilizing multi-frequency structures and internal magnetic coupling. We introduce an internal magnetic-coupled energy harvester (IMC-EH) with a dual-beam structure. In this design, permanent magnets are placed at the free ends of both the inner and outer beams, generating interacting repulsive forces. The IMC-EH is first theoretically simulated to evaluate its performance characteristics. The simulations provide insights into the device's behavior and its potential to improve both the bandwidth and harvesting efficiency compared to conventional EHs. Subsequently, the proposed IMC-EH is fabricated and prepared for experimental verification. The performance of the device is evaluated through practical tests and measurements. These experiments aim to validate the theoretical predictions and demonstrate the effectiveness of the internal magnetic coupling in enhancing the EH's performance.

2. MME coupling model of IMC-EHs

As illustrated in Fig. 1, the proposed IMC-EH design comprises an inner rectangular cantilever and an outer U-shaped cantilever with two branch beams. Each cantilever is composed of a piezoelectric layer (depicted in yellow) and a substrate (depicted in blue). One end of the dual cantilevers is fixed, while the other end is free and equipped with a pair of permanent magnets. The interaction between the inner permanent magnet (IPM) and the outer permanent magnet (OPM) generates mutual repulsion, forming an internal magnetic-coupled structure. This structure introduces a nonlinear magnetic force into the system. In comparison to the external magnetic-coupled structures reported in existing literature,[24] the internal magnetic-coupled structure eliminates the need for additional fixed magnets outside the device. It leverages the interaction force of magnetic coupling, simplifying the device's design. Due to the bistable effect induced by the magnetic coupling, the IMC-EH can exhibit internal magnetic resonance in addition to the inherent resonance of the dual cantilevers. This characteristic enhances the device's bandwidth and improves its output performance.

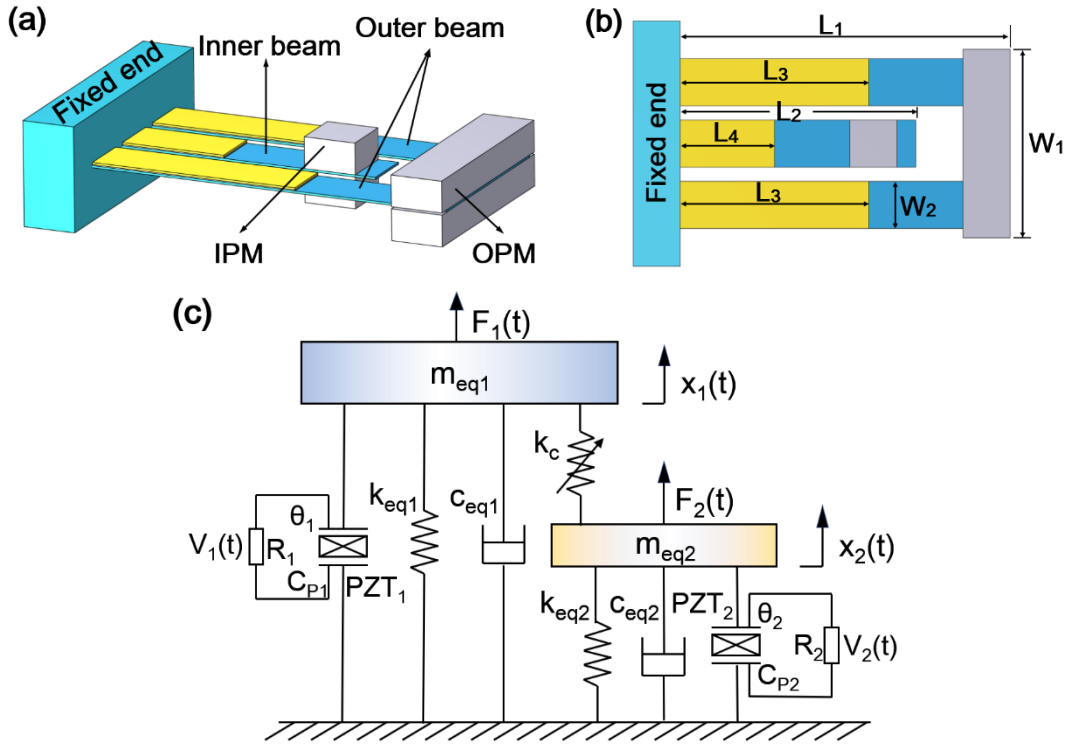

FIG. 1. (a) 3D structural diagram, (b) top view of the IMC-EH, and (c) the lumped parameter MME model of the IMC-EH.

The MME coupling model of the IMC-EH is depicted in Fig. 1(c). In this model, the inner beam is equipped with a piezoelectric element denoted as PZT_1, while the two

outer beams are connected in parallel and equivalent to a single piezoelectric element denoted as PZT_2. The MME model consists of two equivalent masses (m_{eq1} and m_{eq2}), equivalent dampers (c_{eq1} and c_{eq2}), equivalent stiffnesses (k_{eq1} and k_{eq2}), and the two piezoelectric elements. The magnetic force is represented by a nonlinear spring k_c. Within the model, R_i, θ_i, C_{Pi}, and $V_i(t)$ (where i=1, 2) represent the load resistors, equivalent electromechanical coupling coefficients, equivalent capacitances, and the output voltages of the piezoelectric element PZT_i, respectively. $F_i(t)$ represents the force acting on m_{eqi}, and $x_i(t)$ represents the displacement of m_{eqi} relative to their initial positions. The governing equations for the IMC-EH can be expressed as follows:

$$\begin{aligned} m_{eq1}\ddot{x}_1(t)+c_{eq1}\dot{x}_1(t)+k_{eq1}x_1(t)-\theta_1 V_1(t)&=F_{t1}+F_{m1}\\ C_{P1}\dot{V}_1(t)+\frac{V_1(t)}{R_1}+\theta_1\dot{x}_1(t)&=0\\ m_{eq2}\ddot{x}_2(t)+c_{eq2}\dot{x}_2(t)+k_{eq2}x_2(t)-\theta_2 V_2(t)&=F_{t2}+F_{m2}\\ C_{P2}\dot{V}_2(t)+\frac{V_2(t)}{R_2}+\theta_2\dot{x}_2(t)&=0 \end{aligned} \tag{1}$$

These equations describe the motion and interaction of the equivalent masses, dampers, and springs within the IMC-EH system. They provide a mathematical representation of the device's behavior and can be used to analyze its performance and response to external stimuli. The magnetic interaction force F_{mi} (where i=1, 2) in the IMC-EH can be determined using an improved magnetic dipole method.[25] This method involves applying Biot-Savart's law to calculate the magnetic current density of the magnet and combining the total surface charge of the magnetic dipole to obtain the magnetic force between the two magnets. This method provides a way to accurately determine the magnetic interaction force between the inner and outer magnets in the IMC-EH design. It is worthy note that the magnetic interaction force influenced by various factors, including the dimensions and magnetic moment of the magnets, the distance between two magnets, and the tip deflections of the dual beams. The equivalent force produced by the torque of the endmost magnets in the ambient magnetic field is denoted as F_t. The expression for F_t can be given as[5]

$$F_t=wAB_r\varphi(l)H(t) \tag{2}$$

where w, l, A, and B_r are the width, length, projection area, and remnant magnetization of the magnet, respectively. The term "$\varphi(l)$" represents the shape function of the beam

in resonance mode and $H(t)$ is the time-varying external magnetic field acting on the IMC-EH. The interaction between the external magnetic field and the magnets in the device influences the overall behavior and performance of the energy harvester.

According to the MME model shown in Fig. 1(c), the coupled magnetic force F_m in Eq. (1) can be expressed as a function of the equivalent stiffness k_c, which depends on the distance between the two magnets. The presence of both inner and outer magnets leads to the condition $k_c > 0$, indicating that the inner and outer beams are mutually coupled through magnetic forces. However, in the case where there is no magnetic coupling between the two beams, the value of k_c reduces to zero. This implies that the two beams operate as independent vibration systems without any internal magnetic coupling. Such systems without internal magnetic coupling are referred to as Non-IMC-EH (NIMC-EH) systems.

3. Simulation and experiment

The IMC-EH structure depicted in Fig. 1 incorporates a substrate made of beryllium bronze, piezoelectric films composed of $Pb(Zr,Ti)O_3$ (PZT-5H), and two permanent magnets NdFeB. To polarize the PZT layer, a strong DC electric field is applied by two electrodes along its thickness direction. This causes the electric domains within the PZT to align and orient along the direction of the electric field, resulting in the polarization of the PZT layer along the thickness direction. The structure has a total length (L_1) of 35 mm and a width (W_1) of 18 mm. Each beam within the structure has a width of 5 mm. Table I provides the detailed dimensions of the IMC-EH, specifying the dimensions of the substrate and the beams. Table II presents the performance characteristics of the materials used, highlighting the properties of beryllium bronze, PZT-5H, and NdFeB. The IMC-EH structure is analyzed using COMSOL Multiphysics 6.0 that incorporates the coupling of multiple physical fields[26], including solid mechanics, magnetism (without current), magnetism, electrostatics, and circuit. In the current simulation, we select the 'Piezoelectric, Solid' multiphysics in the 'Electromagnetic-Structure Interaction' module, which couples the 'Solid Mechanics' and 'Electrostatics' interfaces and introduces the constitutive relationships required for modeling piezoelectric materials. Additionally, the 'Electrical Circuit' interface is added to combine the 'Electrical Circuit' and 'Electrostatics' interfaces through

terminal settings, enabling circuit connections to the structure. To simplify the calculation process, the magnetic repulsion and torque forces are determined using the improved magnetic dipole method and Eq. (2) instead of simulating the magnetism. The calculated forces, F_m and F_t, are subsequently applied as loads to the end of the cantilever beam, and conventional grid partitioning techniques are employed for the analysis. The structure is analyzed in the frequency domain using the solid mechanics, electrostatics, and circuit physical field interfaces to investigate its characteristics.

TABLE I. Dimensions of the IMC-EH (unit: mm).

Component	Outer beam		Inner beam		OPM	IPM
Material	Cu	PZT-5H	Cu	PZT-5H	NdFeB	NdFeB
Length	L_1=35	L_3=20	L_2=25	L_4=10	5	5
Width	5	5	5	5	20	5
Thickness	0.2	0.2	0.2	0.2	3	5

TABLE II. Material properties of the components.

Property	Beryllium bronze	PZT-5H	NdFeB
Young's Modulus (GPa)	124	56	160
Poisson ratio	0.35	0.36	0.24
Density (kg/m^3)	8900	7500	7600
Piezoelectric constants (m/V)	—	5.93×10^{-10}	—

Figures 2(a) and (b) illustrates the resonance stress distributions of the IMC-EH and NIMC-EH at their first and second order resonances. In both cases, the stress on the inner beam is significantly increased due to the magnetic force between magnets. Consequently, compared to the NIMC-EH, the end transverse displacement of the IMC-EH is approximately 22% higher, as shown in Fig. 2(c).

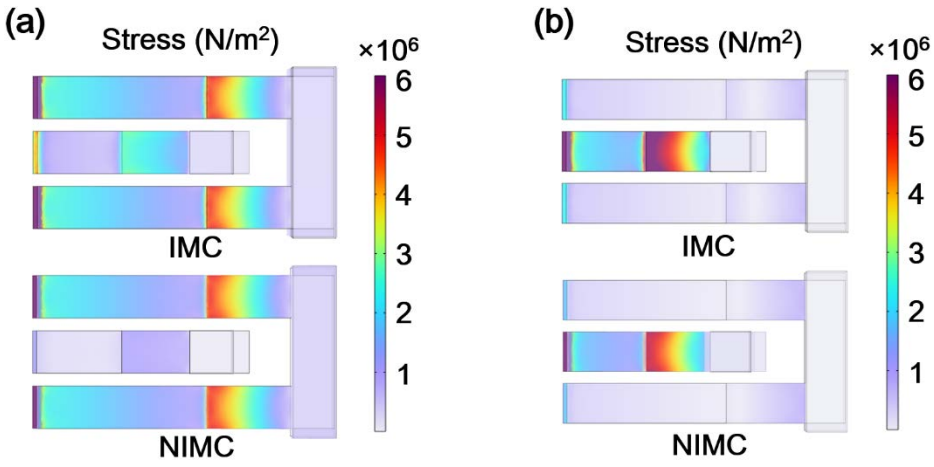

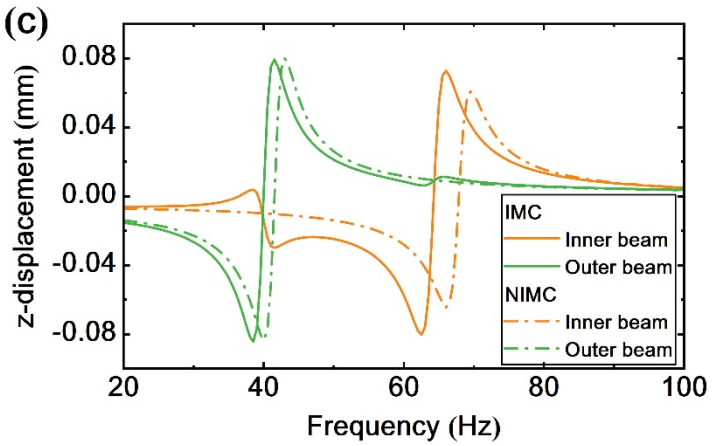

FIG. 2. The stress distributions of the IMC-EH and NIMC-EH at the (a) first-order resonance and (b) second-order resonance. (c) The end transverse displacements of the IMC-EH and NIMC-EH.

To improve the output performance of the proposed IMC-EH, high-elasticity thin copper substrates with the desired shape are manufactured using laser cutting and heat treatment processing techniques. Silver (Ag) electrodes are then deposited on the surface of the piezoelectric ceramics using magnetron sputtering. The piezoelectric ceramic is bonded to the substrate using epoxy resin adhesive through a screen printing process. The assembly is cured in a vacuum chamber at 150 °C and 0.2 MPa for 8 hours. This process results in the formation of a Cu/PZT-5H composite material, as shown in Fig. 3(a). For testing the IMC-EH, a MME test platform is utilized, as depicted in Fig. 3(b). The alternating excitation magnetic field is generated coaxially by a pair of Helmholtz coils driven by a function waveform generator (RIGOL DG1032Z) connected to a power amplifier (SA-PA010). The magnitude of the alternating excitation magnetic field is measured using a gauss meter (Lakeshore 475), while the output voltage of the IMC-EH is measured using a digital oscilloscope (RIGOL MSO5104). During the experiment, the excitation magnetic field is maintained at 1 Oe, and the IMC-EH is positioned at the center of the Helmholtz coil with its axis parallel to the coil's axis. To simulate a real magnetic environment, the magnetic field applied in the experiment is set within the frequency range of 20-100 Hz. This range is chosen as the frequency of environmental stray magnetic fields is generally below 100 Hz.

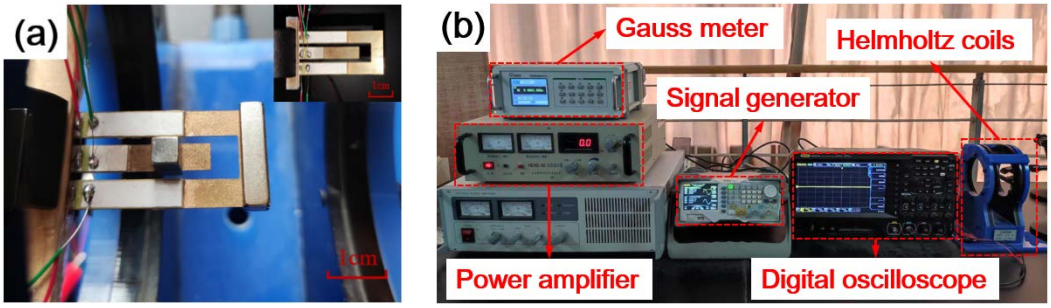

FIG. 3. Photograph of (a) the IMC-EH and (b) the MME test platform.

4. Results and discussion

To validate the improved output performance achieved with the IMC condition, the output voltages of the IMC-EH and NIMC-EH are measured and plotted in Fig. 4. Comparing Figs. 4(a-i) and (b-i), it is evident that both the inner and outer beams of the IMC-EH exhibit internal resonance in addition to their natural resonances at 41 Hz and 62 Hz, respectively. As a result of the magnetic coupling, at the resonant frequency of the inner (outer) beam, the outer (inner) beam demonstrates a noticeable vibration response, even though this frequency significantly differs from its own resonant frequency. Under the IMC condition, the outer beam exhibits a voltage of 1 V at its internal magnetic resonance (62 Hz), which represents a 300% increase compared to the 0.3 V without the IMC condition. Similarly, the inner beam produces a voltage of 1.5 V at its internal magnetic resonance (41 Hz), reflecting a 200% increase compared to the 0.5 V without the IMC condition. These experimental results align well with the simulations, validating the reliability of the findings. Figures 4(a-ii) and (b-ii) illustrates the generated sinusoidal output voltage waveforms from two beams under the applied magnetic field of 1 Oe at their resonance frequencies. Again, it is found that the both beams have available output voltage at the inherent and internal resonance frequencies. Furthermore, the output voltage of the inner beam under the IMC condition has been overall improved across the two resonance frequencies, significantly enhancing the bandwidth. To further broaden the frequency band, the mass of the endmost magnet of the outer beam can be increased to lower its natural resonant frequency, thereby increasing the separation between the internal magnetic resonance and the natural resonance.

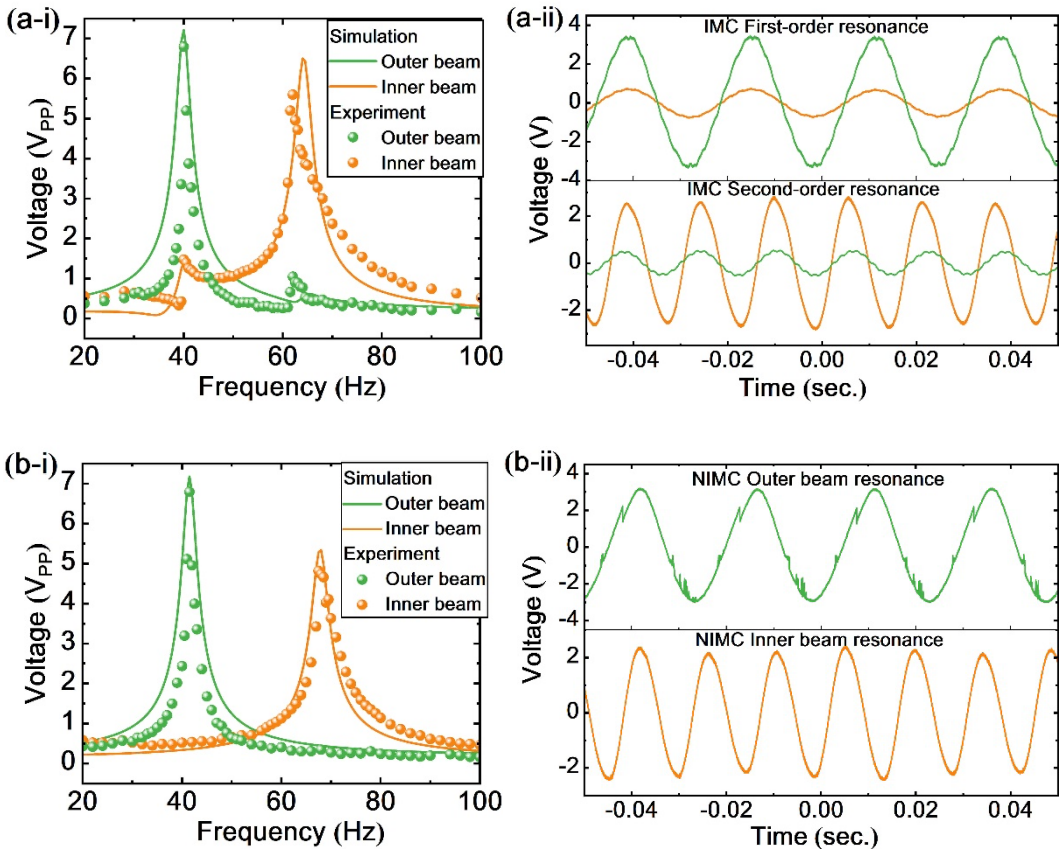

FIG. 4. The output voltages of the (a) IMC-EH and (b) NIMC-EH.

Figure 5(a) illustrates the output voltage of the inner beam under various conditions. The bandwidth of the inner beam with a voltage greater than 1 V is 22 Hz for the NIMC-EH. When two magnets (denoted as 2m) are attached to the end of the IMC-EH, the bandwidth of the inner beam with a voltage greater than 1 V increases to 43 Hz, representing a 95.5% improvement. The bandwidth further increases to 51 Hz, a 132% improvement compared to the NIMC-EH, when the number of endmost magnets is increased to 4 (denoted as 4m). This validates the method of using internal resonance and adjusting the magnets to expand the frequency band. In Fig. 5(b), the total voltage generated by the magnetic harvesters is plotted. When two endmost magnets are added to the outer beam, the total voltage generated by the first-order resonance of the IMC-EH increases from 7.2 V to 8.3 V, a 15.3% increase. Similarly, the total voltage generated by the second-order resonance increases from 5 V to 6.6 V, a 32% improvement. With four magnets added to the end of the outer beam, the total voltage generated by the first-order resonance of the IMC-EH increases by 44.4%, and the total voltage generated by the second-order resonance increases by 32%.

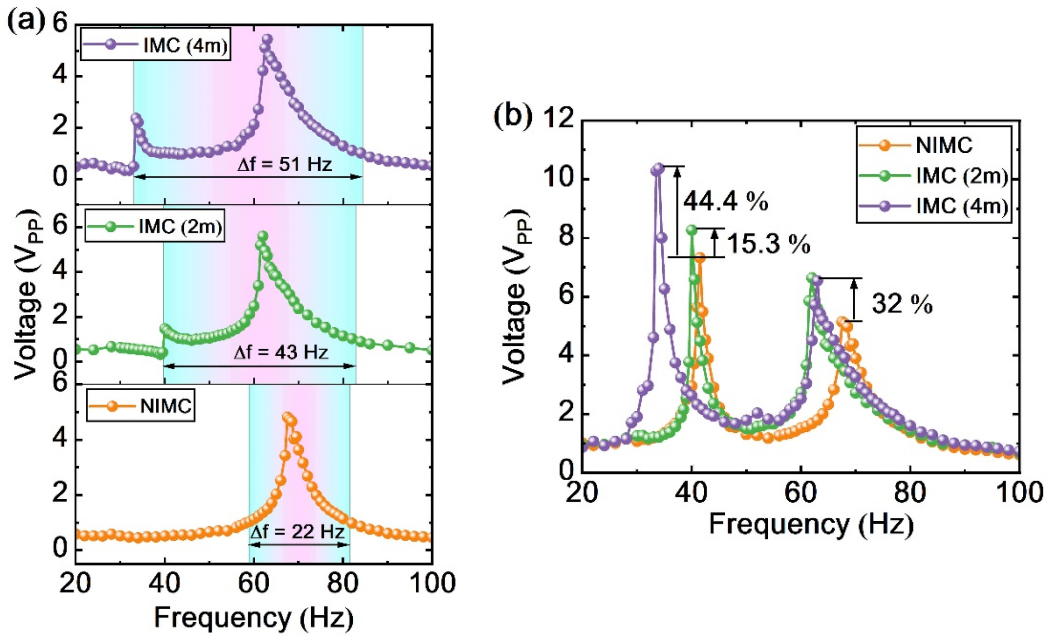

FIG. 5. (a) The output voltages of the inner beam under various conditions. (b) The total voltage of the IMC-EH and NIMC-EH.

By connecting resistors (R_L) to the IMC-EH and measuring the voltage output (U) with four endmost magnets of the outer beam, the output power is calculated using the formula $P=U^2/R_L$. Figures 6(a) and (b) illustrate the power/voltage-load curves of the dual beams at their inherent resonances of 34 Hz and 62 Hz, respectively, under a magnetic field of 1 Oe. The outer and inner beams exhibit maximum powers of 180 uW and 31 μW, respectively, with optimal loads around 200 kΩ and 300 kΩ. Additionally, the inner beam can generate a maximum power of 5 uW under the internal magnetic resonance, as shown in Fig. 6(c). According to the experimental results, the proposed device can generate a maximum power of 1.23 W/m^2 under a weak magnetic filed of 1 Oe. This power is smaller than that generated by commercial photovoltaic cells, primarily due to noticeable differences in operating principles and energy sources. However, when the applied magnetic field increases to 10 Oe, the energy captured per m^2 of the device is expected to reach the same order of magnitude as photovoltaic devices. In practical operation, RMS power, which refers to the calculated equivalent DC power value, is always used to provide a more accurate reflection of the actual power in the AC signal. Figure 6(d) presents the root-mean-square (RMS) output power of different beams. Considering the output power of the structure and its overall volume (approximately 1.6 cm^3, including the piezoelectric film, substrate, and endmost magnet), a maximum RMS output power density of 56.25 μW·Oe^{-2}·cm^{-3} is achieved. It

is noteworthy that the proposed IMC-EH demonstrates a higher output power density compared to previously reported magnetically coupled piezoelectric energy harvesters (36.5 μW·Oe^{-2}·cm^{-3}).[21] The results in Figs. 6(a) and 6(c) demonstrate that the total power of the inner and outer beams, at the inherent resonance, can reach 185 μW even under an ambient magnetic field as low as 1 Oe.

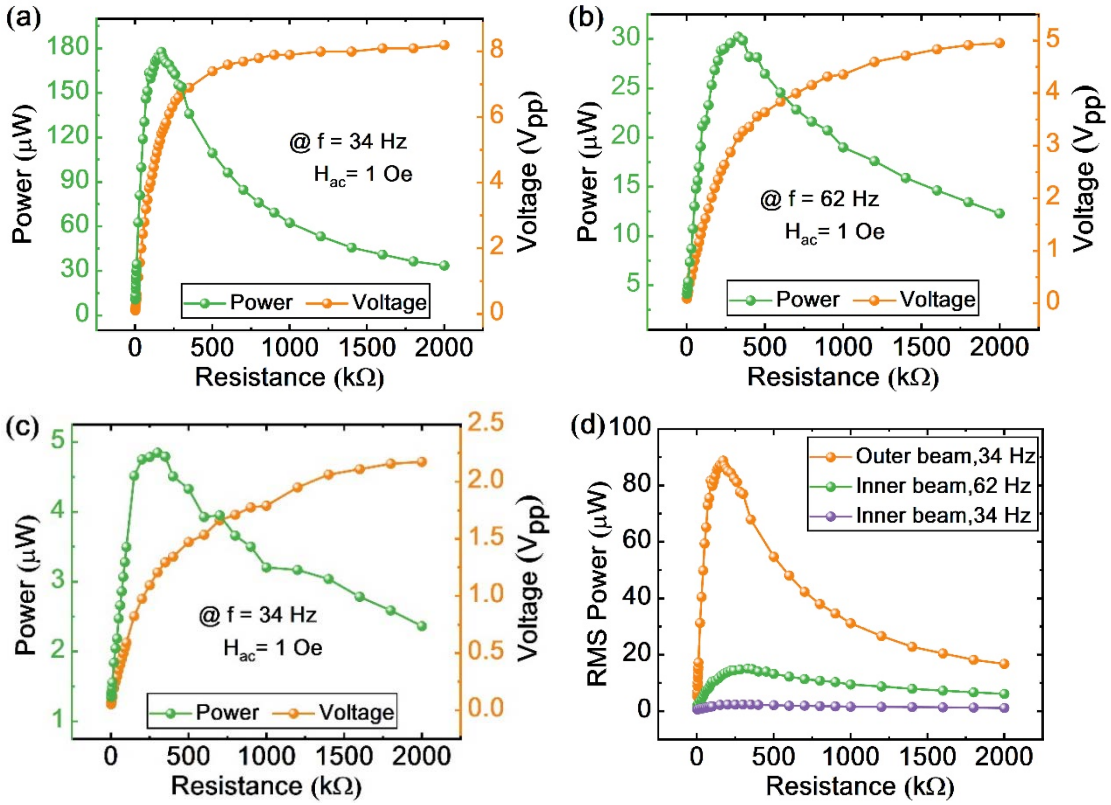

FIG. 6. The output performance of the (a) outer and (b) inner beams at inherent resonance. (c) The output performance of the inner beam at internal resonance. (d) The root-mean-square output power of different beams.

To efficiently utilize the electric energy from the IMC-EH, the generated AC power is first rectified and regulated into DC output through a full-wave rectifier bridge. This DC output is then employed as a standalone power supply to drive a blue light-emitting diode (LED) array, as depicted in Fig. 7(a). In the demonstrations, LEDs are connected in parallel. This parallel connection allows each LED to receive current independently and emit light, which can effectively increase the overall brightness of the circuit. Figure 7(b) demonstrates the practical application of the IMC-EH by continuously powering 26 blue LEDs. This showcases the potential of the proposed MME harvester as a promising solution for operating low-power consumption small electronics.

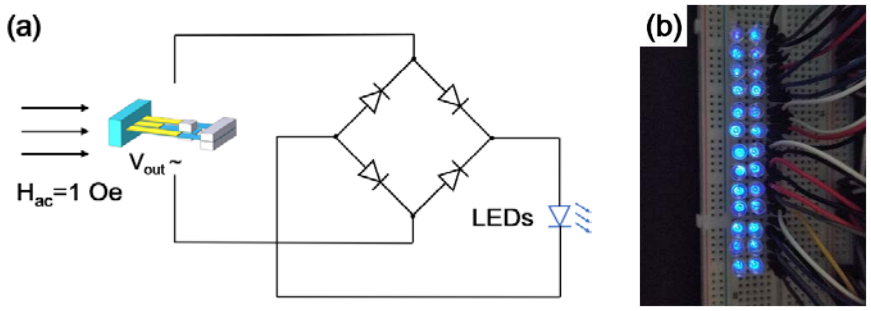

FIG. 7. (a) Schematic of the power management circuit used for driving LEDs. (b) The harvested energy from the MME generator, under a magnetic field of 1 Oe, is sufficient for continuously illuminating 26 5-mm blue LEDs.

Conclusions

In conclusion, this study introduces a novel low-frequency magnetic field EH that utilizes beryllium bronze/Pb(Zr,Ti)O_3 dual-beam structures with tip magnets attached to the inner and outer beams. By incorporating the internal magnetic-coupled (IMC) effect, the EH demonstrates remarkable enhancements in coupling ability and bandwidth. The effectiveness of the IMC mechanism is validated through theoretical formulas and numerical simulations. Leveraging the IMC condition, the proposed IMC-EH achieves an expanded bandwidth, nearly doubling from 22 Hz to 43 Hz. Additionally, the total output voltages at the inherent resonance and internal resonance experience significant improvements of 15.4% and 32%, respectively. Experimental investigations confirm the superior performance of the IMC-EH, surpassing existing magnetically coupled piezoelectric energy harvesters. It achieves a maximum RMS output power density of 56.25 $\mu W \cdot Oe^{-2} \cdot cm^{-3}$. Notably, even under a low magnetic field of 1 Oe, the proposed IMC-EH exhibits a total output power of 185 μW, capable of continuously powering 26 LEDs in real-time. This highlights its potential as a promising solution for low-power consumption in small electronics. Moreover, the findings in this work inspire the design of future self-powered wireless sensor networks within the realm of the Internet of Things. The utilization of the IMC-EH opens up possibilities for autonomous and sustainable operation of low-power devices, contributing to the advancement of energy harvesting technologies.

Acknowledgements

This work was supported by the Natural Science Foundation of Shaanxi Province (No. 2024JC-YBMS-069) and the Fundamental Research Funds for the Central Universities (No. ZYTS23024).

References

[1]A. M. Siddique, S. Mahmud, and B. V. Heyst, Energy Conv. Manag. **106**, 728–747 (2015).

[2]S. P. Beeby, M. J. Tudor, and N. M. White, Sci. Technol. **17**(12), R175–R195 (2006).

[3]J. Ryu, J. E. Kang, Y. Zhou, S. Y. Choi, W. H. Yoon, D. S. Park, J. J. Choi, B. D. Hahn, C. W. Ahn, J. W. Kim, Y. D. Kim, S. Priya, S. Y. Lee, S. Jeong, and D. Y. Jeong, Energy Environ. Sci. **8**(8), 2402 (2015).

[4]V. Annapureddy, S. M. Na, G. T. Hwang, M. G. Kang, R. Sriramdas, H. Palneedi, W. H. Yoon, B. D. Hahn, J. W. Kim, C. W. Ahn, D. S. Park, J. J. Choi, D. Y. Jeong, A. B. Flatau, M. Peddigari, S. Priya, K. H. Kim, and J. Ryu, Energy Environ. Sci. **11**(4), 818–829 (2018).

[5]M. G. Kang, R. Sriramdas, H. Lee, J. Chun, D. Maurya, G. T. Hwang, J. Ryu, and S. Priya, Adv. Energy Mater. **8**(16), 1703313 (2018).

[6]H. E. Lee, J. H. Park, D. Jang, J. H. Shin, T. H. Im, J. H. Lee, S. K. Hong, H. S. Wang, M. S. Kwak, M. Peddigari, C. K. Jeong, Y. Min, C. H. Park, J. J. Choi, J. Ryu, W. H. Yoon, D. Kim, K. J. Lee, and G. T. Hwang, Nano Energy **75**, 104951 (2020).

[7]V. Annapureddy, M. Kim, H. Palneedi, H. Y. Lee, S. Y. Choi, W. H. Yoon, D. S. Park, J. J. Choi, B. D. Hahn, C. W. Ahn, J. W. Kim, D. Y. Jeong, and J. Ryu, Adv. Energy Mater. **6**(24), 1601244 (2016).

[8]H. Song, D. R. Patil, W. H. Yoon, K. H. Kim, C. Choi, J. H. Kim, G. T. Hwang, D. Y. Jeong, and J. Ryu, Energy Environ. Sci. **13**(11), 4238 (2020).

[9]G. X. Liu and S. X. Dong, J. Appl. Phys. **115**, 084112 (2014).

[10]K. Q. Fan, Q. X. Tan, Y. W. Zhang, S. H. Liu, M. L. Cai, and Y. M. Zhu, Appl. Phys. Lett. **112**, 123901 (2018).

[11]Z. H. Yu, Z. M. Li, X. T. Yuan, M. J. P. Asl, and S. X. Dong, Appl. Phys. Lett. **121**(7), 072902 (2022).

[12]J. Q. Gao, Z. C. Sun, H. Dong, Z. Q. Chu, Z. F. Song, and Y. Shen, J. Magn. Magn. Mater. **547**, 168818 (2022).

[13]G. X. Liu, P. H. Ci, and S. X. Dong, Appl. Phys. Lett. **104**(3), 032908 (2014).

[14]X. X. Li, Z. L. Li, H. Huang, Z. Y. Wu, Z. F. Huang, H. L. Mao, and Y. D. Cao, Results Phys. **18**, 103173 (2020).

[15]M. M. Ahmad, N M Khan, and F U Khan, Sens. Actuators A. **344**, 113690 (2022).

[16]S. X. Zhou, J. Cao, D. J. Inman, J. Li, S. S. Liu, and Z. Z. Wang, Appl. Energy. **133**, 33–39 (2014).

[17]H. T. Li, W. Y. Qin, C. B. Lan, W. Z. Deng, and Z. Y. Zhou, Smart Mater. Struct. **25**(1), 015001 (2016).

[18]P. Kim, and J. Seok, Sound Vib. **333**(21), 5525–5547 (2014).

[19]Y. K. Wang, J. Xu, N. Li, and Y. Shi, Eur. J. Mech. A Solids **101** (2023) 105080.

[20]E. Dechant, F. Fedulov, L. Fetisov, and M. Shamonin, Appl. Sci. **7**(12), 1324 (2017).

[21]H. C. Song, P. Kumar, R. Sriramdas, H. Lee, N. Sharpes, M. G. Kang, D. Maurya, M. Sanghadasa, H. W. Kang, J. Ryu, W. T. Reynolds, and S. Priya, Appl. Energy. **225**, 1132–1142 (2018).

[22]E. F. Haghighi, S. Ziaei-Rad, and H. Nahvi, Smart Mater. Struct. **30**(10), 105028 (2021).

[23]S. Y. Liu, L. J. Luo, G. T. Wang, C. Q. Yang, H. Shen, and R. J. Song, Ferroelectrics **614**(1), 201–218 (2023).

[24]B. Chen and X. L. Tang, Proc IMechE Part E: J Process Mechanical Engineering. **235**(2), 162–169 (2020).

[25]G. Q. Wang, W. H. Liao, Z. X. Zhao, J. P. Tan, S. J. Cui, H. Q. Wu, and W. Wang, Nonlinear Dyn. **97**, 2371–2397 (2019).

[26]P. D. Li, X. Y. Li, G. Z. Kang, and R. Müller, Int. J. Mech. Sci. **130,** 203–220 (2017).